GEOPHYSICS, VOL. 63, NO. 6 (NOVEMBER-DECEMBER 1998); P. 2025–2034, 9 FIGS., 1 TABLE.

# Effects of attenuation and scattering on AVO measurements

Adriansyah* and George A. McMechan‡

**ABSTRACT**

The trends and variance in amplitude variation with offset (AVO) observations caused by near-surface structure, attenuation, and scattering are numerically synthesized by pseudospectral viscoelastic 2-D modeling. Near-surface structure produces amplitude focusing and defocusing that significantly distort AVO observations in offset windows at a scale comparable to that of the lateral variations in the structure. Attenuation and scattering decrease absolute amplitudes at all offsets. Scattering and wave interference increase the variance associated with AVO measurements.

Depending on the relative influence of intrinsic attenuation, apparent attenuation associated with scattering, and geometrical focusing, a normalized AVO response can increase or decrease with offset (relative to that for the associated elastic, nonscattering, 1-D solution), and so mimic the behavior predicted as a function of contrasts in density, velocity, porosity or Poisson's ratio. If only relative (normalized) amplitudes are available, it is difficult to distinguish between effects of parameters whose main contributions are to absolute amplitude; for example, a trend of decreasing amplitude (relative to that for an elastic flat-layered model) produced by intrinsic attenuation may be counteracted by focusing/scattering or anisotropic effects over wide aperture ranges. Diagnostic information on AVO effects of scattering and attenuation is lost when the noise level is sufficiently high. Interpretations of AVO observations based on homogeneous layered elastic models must therefore be used with caution as they are, in general, nonunique. Lateral variations in AVO parameters are the key to detecting hydrocarbons, so lateral changes in AVO produced by lateral changes in the overburden properties have potential for being misinterpreted, especially if the recording aperture is small.

## INTRODUCTION

Amplitude variations with offset (AVO) have been successfully used as direct hydrocarbon indicators because they are a function of the contrast in rock and fluid properties across an interface (e.g., Ostrander, 1984; Chacko, 1989; Rutherford and Williams, 1989; Snyder and Wrolstad, 1992; Allen and Peddy, 1993; Castagna and Backus, 1993; Santoso et al., 1995; Landro et al., 1995).

Appropriate interpretation of absolute AVO information can be made in terms of the reflectivity behavior of the target only if other offset-dependent amplitude effects are adequately accounted for (Toksöz et al., 1979; Martinez and McMechan, 1991; Castagna, 1993a). This is usually done empirically rather than deterministically by approximately removing all the effects of layers overlying the target by considering only differences between the target reflection and a nearby reference reflection (Chiburis, 1984, 1987, 1993; Allen and Peddy, 1993). Even this does not guarantee success because the reference layer may itself generate wave conversions and artifacts that overlie and distort the target reflection (e.g., Ross, 1991). In the examples below, we use the reflection from the target interface in a model in which the overlying material is homogeneous and purely elastic as the reference to study the AVO deviations produced by shallower variations. When lateral variations in the overburden are small or are sufficiently well known that ray-tracing can be used to obtain angles of incidence, procedures such as the weighted stacking of Smith and Gidlow (1987) become viable. To understand the strengths and limitations of these methods, it is important to investigate propagation and scattering effects in the overburden (Martinez, 1993) as well as the properties of the target (e.g., Juhlin and Young, 1993) and background noise (Ross, 1991, 1992; Rutherford, 1993; Drufuca and Mazzotti, 1995).

Manuscript received by the Editor September 27, 1996; revised manuscript received May 4, 1998.
*The University of Texas at Dallas, Center for Lithospheric Studies, P.O. Box 830688 (FA31), Richardson, TX 75083-0688 and Pertamina Indonesia, Exploration and Production Division, Jl. Merdeka Timur 6, Jakarta 10110 Indonesia. E-mail: ancha@utdallas.edu.
‡The University of Texas at Dallas, Center for Lithospheric Studies, P.O. Box 830688 (FA31), Richardson, TX 75083-0688. E-mail: mcmec@utdallas.edu.

Neglecting any systematic amplitude factor will bias the estimated properties of the target. Neglecting any random amplitude factor will change the variance associated with the estimated properties. If the model parameterization is inappropriate for the data, the observations will be attributed erroneously to a distorted combination of those factors that are present in the model.

Castagna (1993a, b) and Castagna et al. (1995) discuss various factors that affect seismic amplitude. These include instrument responses, source/receiver coupling, spherical divergence, anelastic attenuation, anisotropy, the presence of fluids, 3-D and off-line effects, and near-surface scattering and inhomogeneities. Widmaier et al. (1996) and Kan and Young (1993) illustrate the effect of a finely layered overburden on AVO. Samec and Blangy (1992), Luh (1993), and Kang and McMechan (1993a, b) discuss attenuation effects. Xu et al. (1993) and Kim et al. (1993) discuss the influence of vertical velocity gradients and anisotropy in the overburden. Kang and McMechan (1994) and Chang and McMechan (1996) investigate the interaction of intrinsic attenuation and apparent attenuation associated with scattering. Bourbié and Nur (1984), Juhlin and Young (1993), and Simmons and Backus (1994) show the effects of anelasticity and fine layering of the target zone on AVO. Wave propagation effects can be of the same magnitude as AVO variations in reflections (e.g., Simmons and Backus, 1996) and lead Samec and Blangy (1992) to suggest that a model based approach has value. This statement was also supported by the results of Martinez and McMechan (1987, 1991) and Martinez (1993). Controlled amplitude processing (Yu, 1985) may also be used to compensate for near-surface and overburden effects.

If the near-surface structure and the overburden properties can be accurately estimated, an approach to isolation of their effects is to calculate and compare the responses of models with and without them present. In the examples below, we take this approach to study the nature and magnitude of near-surface and overburden effects in a series of examples for models that include the effects of structure, viscoelasticity, and scattering. The combined effects of near-surface geometry, attenuation, and scattering on AVO have not previously been investigated.

## MODELS AND SYNTHETIC DATA

### Model geometry and parameterization

The three model geometries considered are shown in Figure 1. Each consists of a flat reflector, overlain by overburden that is homogeneous (Figure 1a), or with a surface layer that is either flat (Figure 1b) or is geometrically more complicated (Figure 1c). These model geometries are referred to below as models A, B, and C, respectively. For specific examples, the models are either purely elastic or have viscoelastic and/or scattering regions. Model parameters are given in Table 1.

**Table 1. Layer parameters for models A, B, and C of Figure 1.**

| | $V_p$ (km/s) | $V_s$ (km/s) | Density (g/cm$^3$) | $Q_p$ | $Q_s$ |
|---|---|---|---|---|---|
| Surficial layer | 1.8 | 0.52 | 0.202 | 60 | 23 |
| Overburden layer | 2.2 | 0.83 | 0.212 | 73 | 37 |
| Target layer | 3.2 | 1.68 | 0.233 | 105 | 74 |

Two-dimensional scattering is introduced using a 2-D von Karman distribution (e.g., Frankel and Clayton, 1986; Crossley and Jensen, 1989) with a deviation of 20% in all model parameters with a correlation distance of 50 m, which corresponds to approximately 0.8 $P$-wave wavelengths at the dominant frequency of 30 Hz. Thus, this is near the peak of $P$-wave scattering efficiency (e.g., Blair, 1990; Tang and Burns, 1992). One-dimensional scattering (by a layered sequence) is similarly defined, but material properties vary only vertically.

### Numerical simulation and AVO measurements

For numerical simulation of the responses, the models (Figure 1) were gridded with a 20-m spacing in both horizontal and vertical directions (256 × 128 points, which includes absorbing boundaries on all four sides of the grid). All references to positions below are exclusive of the absorbing boundary portions of the grid. Both source and receivers lie at the surface of the model. The source is a pressure pulse with a 30-Hz Ricker time wavelet located at the left edge of the model, and there are 96 receivers spaced at 40 m. Since the models are 2-D, the source is a line perpendicular to the model plane. Although both vertical and horizontal displacement components are generated in the simulation, only the vertical displacements of the $P$-wave reflection from the reflector at 1.24 km depth will be considered below. The combination of the shallow reflector and the long recording offsets produce postcritical as well as precritical reflections. Postcritical reflections are particularly sensitive to velocity contrasts. Both $P$-$P$ and $P$-$S$ postcritical reflections have been previously used in exploration, primarily because they have larger signal-to-noise ratios than precritical data (e.g. Poley, 1964; Schultz et al., 1983; Winterstein and Hanten, 1985; Chiburis and Al-Faraj, 1987), so it is of interest to include them here.

For analysis of strong bright spots (such as those associated with changing from brine to gas) for which the reflectivity is primarily controlled by the elastic properties, the use of elastic reflection coefficients (e.g., Koefoed, 1955) or derived approximations (e.g., Shuey, 1985) are often useful (e.g., Allen and Peddy, 1993; Smith and Gidlow, 1987; Estill and Wrolstad, 1993). However, when more accurate solutions are required, or when the contrasts in elastic properties are less, other factors (such as attenuation and anisotropy) become important (Bourbié and Nur, 1984; Castagna et al., 1993, 1995; Martinez and McMechan, 1991; Shapiro et al., 1994; Shapiro and Hubral, 1996). Thus, for the examples below, the pseudospectral viscoelastic forward modeling technique described by Kang and McMechan (1993a) was used to calculate synthetic responses of the models. The algorithm is based on the work of Reshef et al. (1988) and Kang and McMechan (1990), with the inclusion of viscoelasticity using memory variables following Carcione et al. (1988) and Tal-Ezer et al. (1990). We neglect the effects of free surface reflection by defining the surface to be an absorbing boundary. Since most of the examples below involve differences from a reference AVO response and the free surface effect would be approximately equal in the two responses in the subtraction, the conclusions are not significantly altered by its omission.

To avoid NMO stretching, reflector flattening (applied for convenience in plotting) involved a simple bulk shift of all trace samples determined by the NMO curve for the time of the maximum positive reflection amplitude at zero offset. The AVO measurements were simply the maximum positive peak

amplitude in the wavelet of each trace, and so are unaffected by residual moveout after time shifting. As our AVO analysis is based on relative amplitudes, postcritical phase shifts are not explicitly considered. Divergence corrections were not applied because these also have minimal effect on amplitudes relative to those in the response of the reference model, and it is not possible to do accurate corrections for those data that contain complicated scattering or even for simpler situations such as for interference between closely spaced reflections from a sequence of reflectors.

To illustrate the processing under ideal conditions, consider the response of model B (Figure 1b) as shown in Figure 2. To get a reflection from the interface that is free of interference by direct $P$- and $S$-waves, mode conversions (and free surface multiples and surface waves if a free surface was used), and numerical artifacts that might interfere with the event to be analysed (e.g. Ross, 1991), synthetic responses were calculated twice for each model, once with and once without the target reflector. Then, AVO measurements (Figure 2c) were made on the residual (Figure 2b) after subtraction of those two responses. For real data analysis, this subtraction would be replaced by some form of wave separation to reduce interference between the target reflection and all other waves (e.g., Ross, 1991). For the example in Figure 2a, a slowness filter would be effective because the interfering waves have steeper trajectories than the target reflection. $f$-$k$ filtering, coherency filtering in short windows, or wave-equation-based wave separations (e.g., Sun and McMechan, 1991) can be used as appropriate, but operations such as automatic gain control that do not preserve amplitude are to be avoided (e.g., Allen and Peddy, 1993). The consequence of not reducing coherent noise is illustrated in Figure 2c; local increases in amplitude variance are associated with wave interference.

AVO measurements are normally made only on data with short offset/depth ratios, but there are useful variations in information content, especially at larger ratios (e.g., Todd and Backus, 1985). For reference in the wider aperture results presented below, the position of offset/depth = 1 (1.24 km), and the offset of the critical reflection (2.34 km) for the reference model A (Figure 1) are identified in Figure 2.

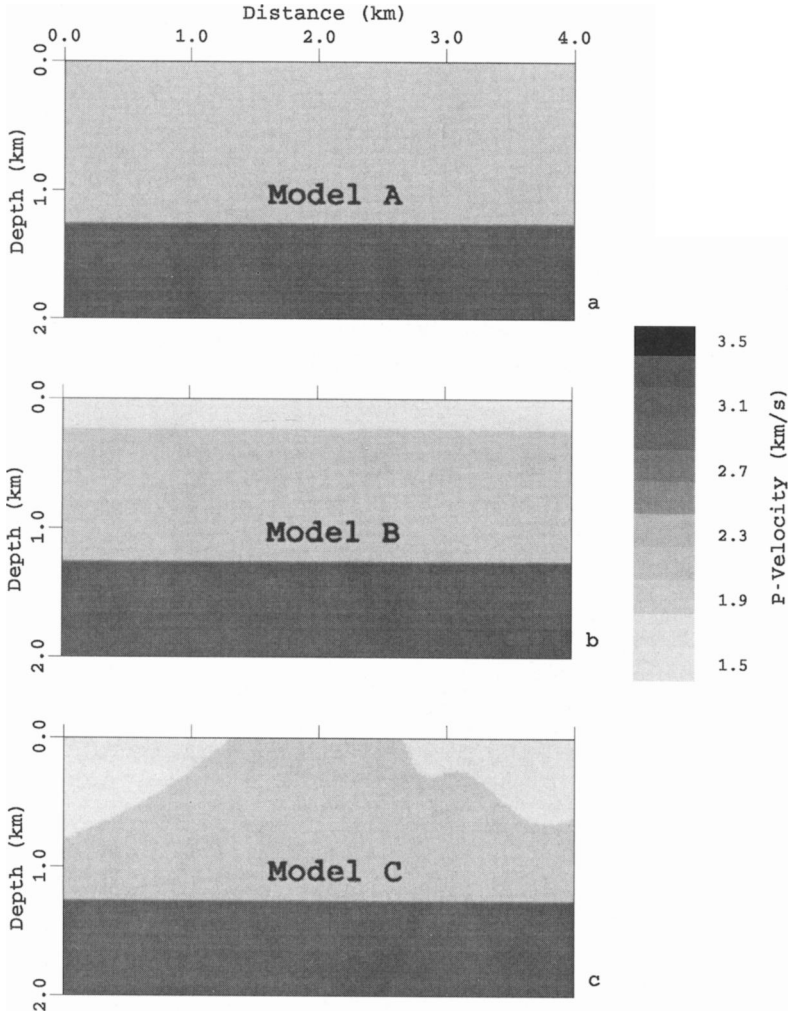


FIG. 1. Three progressively more complicated models used to generate test data. Viscoelasticity and scattering are also added for later examples. Model parameter values are given in Table 1. Models shown are exclusive of the absorbing boundaries.

## EXAMPLES AND ANALYSIS

In this section, we present results for AVO computations for the single flat reflector at 1.24 km depth in the three models in Figure 1. The effects of overburden geometry and scattering are considered for both elastic and viscoelastic models. For computational efficiency, common-source (rather than common-midpoint) gathers are generated and analyzed; this does not affect the conclusions. The pure elastic, nonscattering responses are used as the basis of comparison.

### AVO effects of near-surface geometry in elastic media

The reflections from the reflector at 1.24 km depth in the pure elastic models (Figure 1), after flattening and subtraction of interfering arrivals, are shown in Figure 3. The AVO curves for the data in Figure 3 are in Figure 4; the AVO curves are presented in three ways. The relative amplitudes (Figure 4a) show similar trends for all three models. However, the reflection amplitudes for models B and C (which have the low velocity surface layers) have higher amplitudes because the low velocity bends the rays more steeply, thereby increasing the amplitude of the vertical component; this effect is more pronounced as offset (and hence the incident angle at the base of the surface low-velocity zone) increases. The postcritical amplitude variations in curves A and B are the result of interference between the reflection and the head wave.

In Figure 4b, the AVO data are plotted as percent deviations from model A to emphasize the differences. At the distances corresponding to precritical reflections (<2.34 km), there is an increasing difference between the responses of models A and B (from 5% at zero offset to 35% at 2.5 km offset) because of the ray-bending effect discussed in the previous paragraph. Over

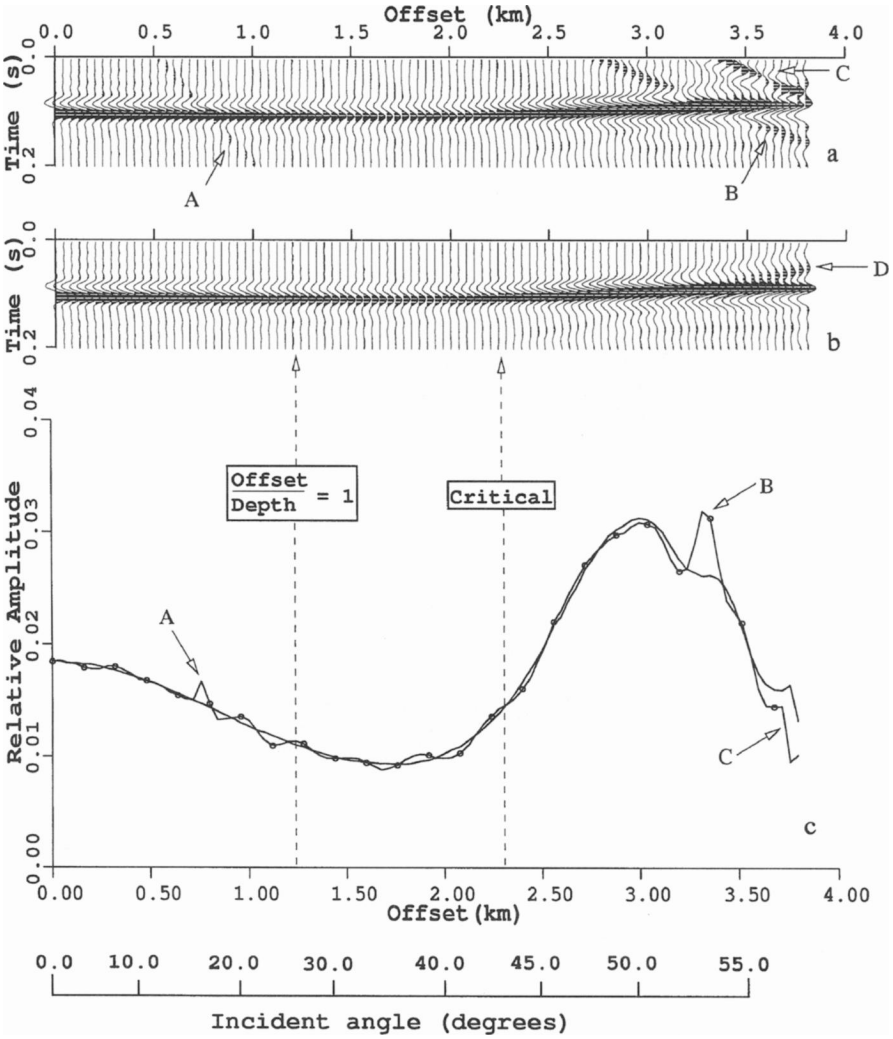


FIG. 2. AVO measurements for the reflector at 1.24 km depth in Figure 1b. (a) is the reflection after flattening. Arrivals A, B, and C are various source-generated interfering waves. (b) is the same as (a), after subtraction of the interfering waves. The critical reflection is at 2.34 km offset; D is the head wave from the interface. Times in (a) and (b) are relative; the absolute zero-offset reflection time is 1.16 s. (c) contains the AVO curves for the data in (a) (the curve with symbols) and for the data in (b) (the curve without symbols). In (c), and all the following amplitude plots, the amplitude scale is arbitrary [as amplitudes in (a) and (b) depend on the source strength used in the simulations], but both curves have the same scaling and so can be directly compared. The deviations A, B, and C in (c) are caused by the similarly labeled interfering waves in (a).

the same offset range, the difference between the responses to models A and C has larger local variations, but no consistent trend. The large peak near 3.1 km offset in the curve for model C is the result of geometrical focusing by the curved interface at about 0.3 km depth and 2.8 km distance in the model (see Figure 1c). Corresponding time statics are also clearly visible in the data for model C (Figure 3c).

Most AVO measurements involve only relative amplitudes or amplitude anomalies (e.g., Chiburis, 1987; Castagna, 1993a; Simmons and Backus, 1996) because absolute values of some effects (including the initial source strength and directivity, overburden anisotropy, 3-D structure, etc.) are often not available. Figure 4c shows deviations that are similar to those in Figure 4b, but computed from data that are normalized to the zero-offset amplitude for reference model A. This is closer to the format that would normally be available for field data. Normalization can be to any desired reference. Another option for the reference would be the average amplitude; in this case, the results would vary with the offset aperture.

### AVO effects of near-surface scattering and attenuation

Figure 5 contains time-shifted reflections from the reflector at 1.24 km depth in model B for six different combinations of attenuation and 2-D random scattering after interference subtraction. The suites of AVO curves in Figure 6a extracted from the data in Figure 5 show a decrease of absolute amplitude with increasing attenuation (decreasing $Q$); curves 1, 2, and 3 are for progressively greater attenuation. There is also an offset-dependent amplitude decrease in curves 2 and 3 relative to the elastic case (curve 1) (see Figure 6b). This decrease is a consequence of amplitudes at larger offsets having longer travel paths, and hence more attenuation. In curve 2 (Figure 6b), the amplitude decrease with offset is not proportional to the increase in total path length because only the upper layer is attenuating, and the change in path length in this layer is relatively small with increasing offset because of the ray bending that occurs at its base. Larger differences would be present if the path lengths were greater or the $Q$ values were smaller. The presence of finite $Q$ also changes reflection and transmission coefficients from the corresponding elastic values (e.g., Martinez and McMechan, 1987).

The responses for the models that combine attenuation and 2-D scattering (curves 4, 5, and 6) also have progressively lower amplitudes with increasing attenuation, but they have consistently lower relative amplitudes and larger variance than the corresponding attenuation-only responses (Figure 6b). The lower relative amplitudes are produced by the apparent attenuation associated with scattering (e.g., Chang and McMechan, 1996), and the higher variance is produced by the local focusing and defocusing of energy and by interference between the scattered waves. The latter was previously illustrated in Figures 2 and 4.

Another form of scattering that has received recent attention is from a thinly layered (1-D) sequence (Juhlin and Young, 1993; Shapiro et al., 1994; Sams, 1995; Shapiro and Hubral, 1996; Widmaier et al., 1996). To investigate this in the present context, the overburden in model A and the surficial layer in model C were replaced by a sequence of thin horizontal layers with the same statistics used in the 2-D scattering (but only in 1-D). The results are shown in Figure 7. For model A (Figure 7a), the scattering response (curve 2) differs most from the nonscattering response (curve 1) at zero offset. This is consistent with the results of Widmaier et al. (1994) and is a consequence of the layering-induced anisotropy and of decreased transmission losses (decreased effective attenuation) with increasing offset. The same overall behavior is seen in the responses of model C (Figure 7b), but is significantly modified by the varying thickness of the surficial layer. The curves for the scattering and nonscattering models are very close together at offsets between 0.8 and 2.5 km, where the surficial layered

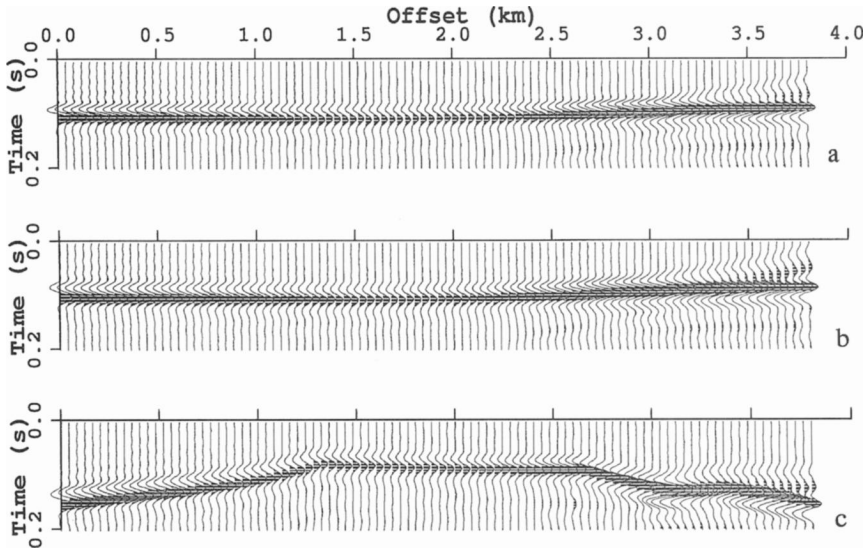


FIG. 3. Reflections, after flattening and interference subtraction, for the three elastic models in Figure 1. (a) is for model A, (b) is for model B, and (c) is for model C. Times are relative; the absolute zero-offset time is model-dependent, with an average of 1.2 s. The corresponding AVO curves are in Figure 4.

sequence is thin or absent (Figure 1). The near-surface geometry (focusing) effect is sufficiently strong that it masks the AVO signature of the target reflector over large offset ranges that correlate with the geometry of the surficial layer.

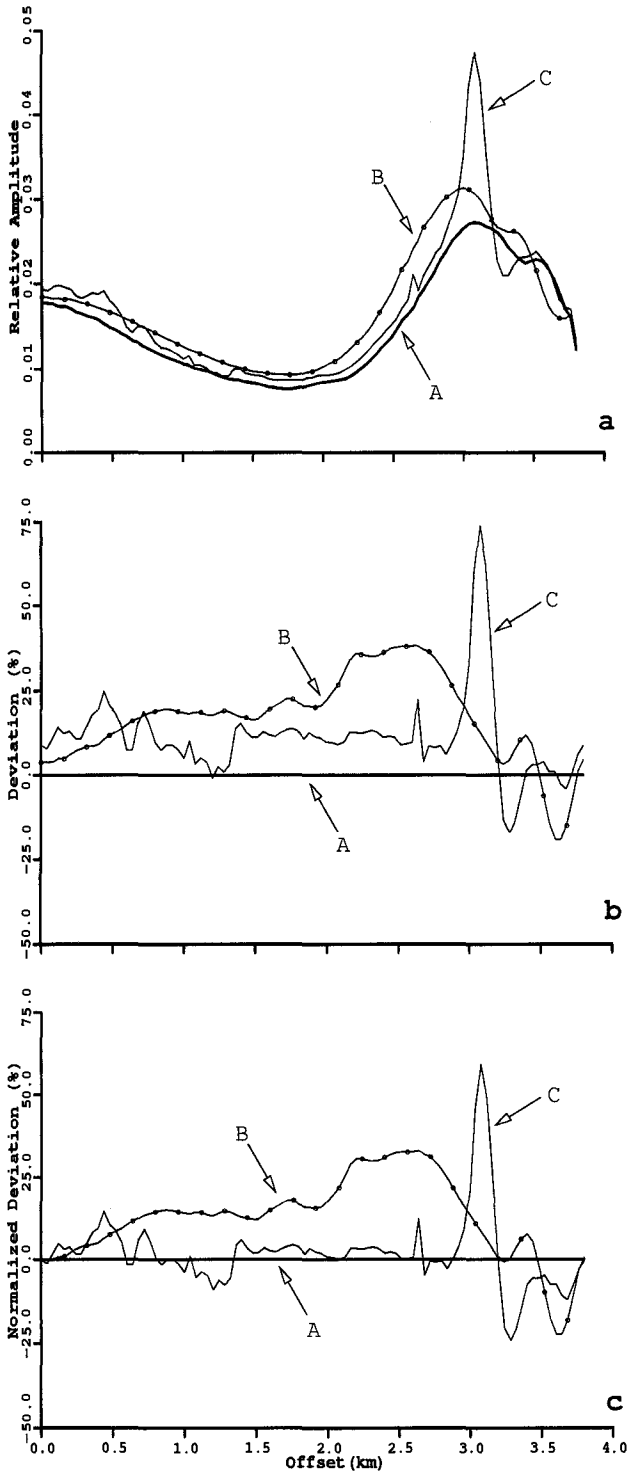


FIG. 4. AVO curves for the data in Figure 3. Curves are labeled to correspond to the similarly labeled models in Figure 1. (a) are the relative amplitudes after flattening and interference subtraction, (b) are the deviations from model A, and (c) are the deviations from model A after normalization of the data to the amplitude for model A at zero offset.

### Effects of data preprocessing on AVO measurements

In all the examples above, data preprocessing has included subtraction of all interference produced by the source and extraneous waves generated above the reflector. The effects of the overlying material on the reflection itself are not changed by this subtraction. As scattering in the overburden increases, however, the reflection becomes increasingly obscured in the raw data. This indicates that diagnostic information on scattering and attenuation is lost when the noise level is sufficiently high. Thus, it is important to investigate the effects of the data preprocessing on the results.

Figure 8 contains the windowed, flattened reflections from the reflector at 1.24 km depth in model C, after interference subtraction, with the same combinations of attenuation and scattering that were considered in Figure 5 for model B. Figures 9a and 9b contain the AVO deviation curves normalized to the zero-offset amplitude of reference curve 1 for the data with and without interference subtraction, respectively. Interference subtraction has significantly reduced the AVO amplitude variations.

In both Figures 9a and 9b, there is a higher variance in the offset ranges $<1.3$ km and $>2.6$ km. These ranges correspond to receivers lying within the low velocity, surficial scattering region. Between these, the AVO curves are relatively smooth. The explanation of this difference is that a wavefront propagating from a scattering zone into a homogeneous zone has a "self-healing" property, becoming more coherent as a consequence of Huygen's principle.

Measured AVO responses are often smoothed before interpretation to minimize the effects of local variations caused by wave interference and scattering. Thus, smoothing, at least to some extent, can be substituted for interference subtraction and does not require explicit information on the details of the model. Figure 9c contains the same data as in Figure 9b after smoothing and normalization. Consider the normalized amplitudes at short offsets ($<1.0$ km) in Figure 9c. Depending on the relative influence of attenuation, scattering, and local focusing, the AVO deviation can increase or decrease with offset, relative to that for the elastic, nonscattering, flat-layered response. This behavior has previously been associated with the contrast in Poisson's ratio or density (Ostrander, 1984), impedance (Rutherford and Williams, 1989), porosity (Chacko, 1989; Snyder and Wrolstad, 1992), or anisotropy (Kim et al., 1993) across an interface.

Another salient observation in Figure 9c is that the range in percent deviations at postcritical distances ($>2.34$ km) is similar to that at most precritical distances. This is because amplitude changes produced by both intrinsic attenuation and scattering mechanisms are proportional to the incident amplitude. This is also seen in Figure 6a, where both the absolute amplitude decrease produced by intrinsic attenuation and the variance increase produced by scattering effects are less where amplitudes are low (e.g., 1.0 to 1.5 km offset) than where they are high (e.g., 2.5 to 3.5 km offset).

## DISCUSSION AND CONCLUSIONS

Although much success has been experienced in AVO analyses in some environments, there are also situations in which it appears to be less than reliable. The latter may be a consequence of oversimpified assumptions that neglect factors that

are important, resulting in AVO interpretations that are biased and leading to erroneous conclusions. We have shown that near-surface effects may mimic the AVO behavior expected from petrophysical contrasts at deeper reflectors and so should either be compensated for or included in the model as part of AVO analysis. Perhaps the most revealing perspective is achieved by noting that the wide variety of AVO responses considered in this paper are all from the same flat reflector. The most important cause of AVO data distortions is lateral variations of the material properties in the overburden.

We have concentrated in this study on the vertical component of the displacement of compressional waves. However, the same processes will similarly affect all components, and shear and mode-converted reflections. Particle velocity is the time derivative of displacement and so is equivalent in terms of information content. Pressure responses in marine data would not have as strong a decrease of amplitude with increasing incident angle at the receiver that is present in the vertical component responses of land data as simulated here.

The examples presented above are an important part of, but are still not, the complete picture. We have concentrated on near-surface effects, limiting ourselves to layer geometry, attenuation, and scattering, while neglecting free-surface topography, off-line (3-D) effects, and (with the exception of 1-D scattering in the overburden) complexities generated by deeper features lying between the reflector and the sources and receivers. We have also omitted discussion of the interaction of these parameters, which can also have important consequences for amplitudes (e.g., Chang and McMechan, 1996). The computational tools for investigation of a more complete parameterization are available (e.g., Dong and McMechan, 1995), but are correspondingly more expensive to use.

A number of conclusions can be drawn from the examples. It is difficult to separate behaviors produced by intrinsic attenuation from those produced by anisotropy or scattering, which have very different absolute amplitude signatures but which may have very similar relative AVO signatures over wide aperture ranges. Amplitude normalization is convenient for display purposes and it preserves trends within individual AVO curves, but one cannot compare two normalized AVO curves and infer anything about their relative amplitudes. Still, trend information is valuable and may be extracted from normalized data [e.g., the ratio of AVO gradient to zero-offset amplitude ("B/A") is widely used (e.g. Chiburis, 1987; Luh, 1993)].

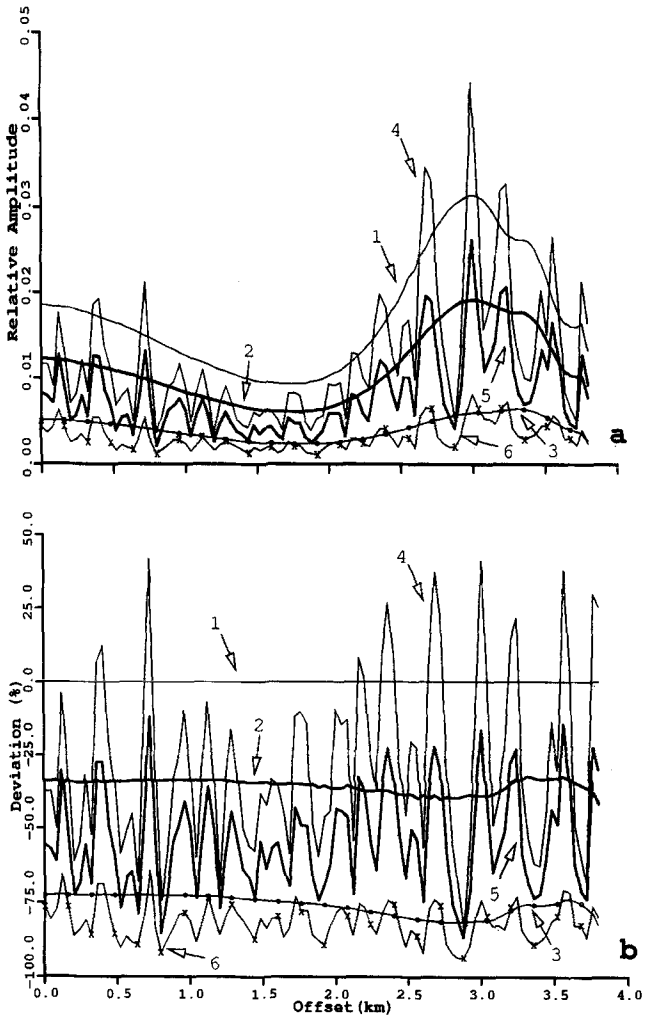


FIG. 6. AVO responses for six configurations with the geometry of model B in Figure 1. In each panel, curves 1 through 6 correspond to the data in Figures 5a through 5f, respectively.

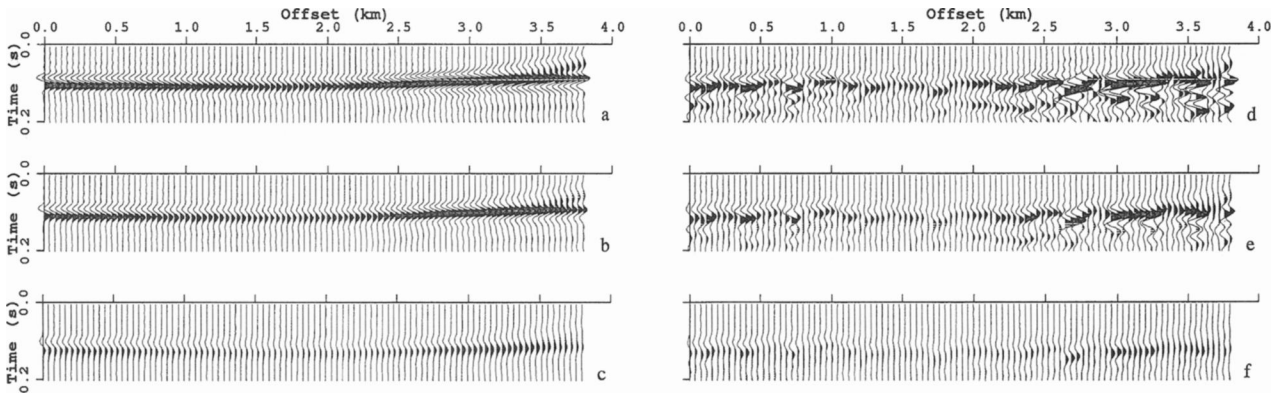


FIG. 5. Common-source responses of model B. The left column shows responses as a function of attenuation only; the right column, as a function of scattering and attenuation. (a) is the pure elastic response; (b) and (c) are the viscoelastic responses for attenuation in the surficial layer only, and in both the surficial and overburden layers, respectively. (d) is the pure elastic response including scattering in the surficial layer; (e) and (f) are the responses of the same viscoelastic models used to compute (b) and (c), respectively, with the inclusion of the same scattering as in (d). Times are relative; the absolute zero-offset time is model dependent, but is approximately 1.16 s.

Absolute average amplitudes are decreased with offset (compared to those for the nonscattering, nonattenuating model) by both attenuation and scattering (and by the fact that we are using only vertical displacements). On the other hand, normalized amplitudes (relative to that at zero-offset) are consistently decreased with offset by attenuation, and may be increased or decreased with offset by local focusing or scattering. Scattering increases the variance in AVO measurements. Near-surface geometrical focusing/defocusing can act over large offset ranges and can produce different apparent AVO deviation trends in different offset ranges, so it is necessary to have sufficient aperture. All of these near-surface effects individually and/or collectively can mask, mimic, or distort the true AVO associated with deeper targets. Lateral variations in AVO parameters are the key to detecting hydrocarbons, so lateral changes in AVO produced by lateral changes in the overburden properties have potential for being misinterpreted. On the other hand, as long as a problematic overburden is laterally invariant and the hydrocarbon AVO anomaly is sufficiently strong, relative responses will be a viable exploration tool.

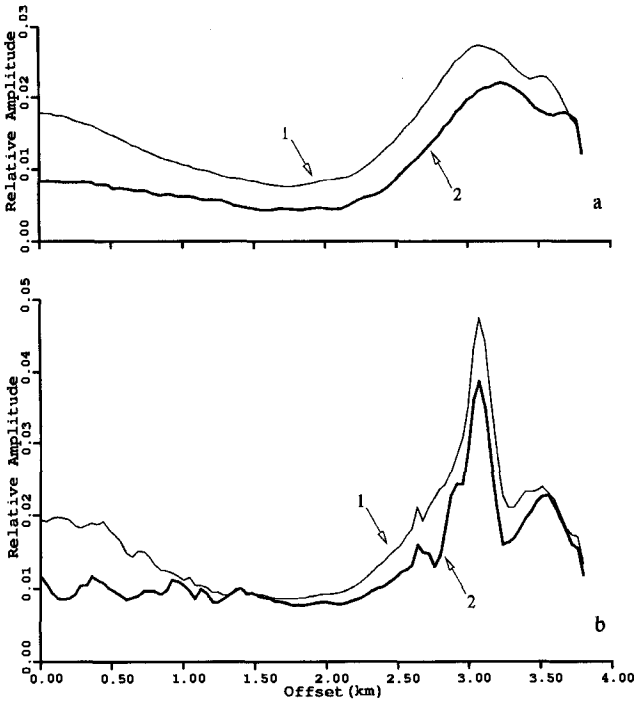


FIG. 7. AVO responses with and without scattering produced by a sequence of thin layers within (a) the overburden layer of model A and (b) the surficial layer of model C. Lines (1) are for the responses without scattering; lines (2), with scattering. All responses are with interference subtraction.

Although we have illustrated the types and magnitudes of near-surface effects to be expected, we have not explicitly shown how to deal with them. Ideally, the problems may be avoided by using data from regions that are relatively free of scattering, attenuation, and distortions produced by near-surface structure so that rays may be confidently traced through the overburden (as was done by Smith and Gidlow, 1987) or by using only amplitudes relative to a reference reflection (Chiburis, 1987; Castagna, 1993b). The results above show that, whereas a deterministic prediction and correction of AVO anomalies originating in the near-surface and overburden is difficult and may not be practical, it is neccessary to consider the type and magnitude of these effects that are present as part of choosing a viable method of AVO analysis for any particular data set.

## ACKNOWLEDGMENTS

The research leading to this paper was supported by PERTAMINA, Indonesia, by the Petroleum Research Fund of the American Chemical Society, under Grant 29911-AC2, and by the sponsors of the UT-Dallas Geophysical Consortium. The authors appreciate constructive reviews by M. M. Backus and J. L. Simmons. This paper is Contribution No. 890 from the Geosciences Department at The University of Texas at Dallas.

## REFERENCES

Allen, J. L., and Peddy, C. P., 1993, Amplitude variation with offset: Gulf Coast case studies: Soc. Expl. Geophys., Geophys. Dev. Series **4**.

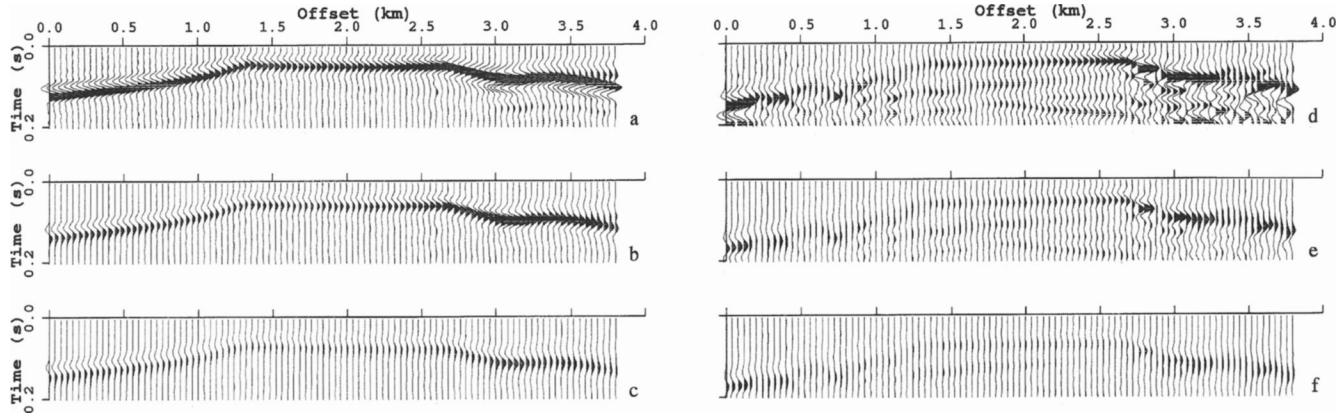


FIG. 8. Common-source responses of model C with interference subtraction. The left column shows responses as a function of attenuation only; the right column, with scattering in addition to the attenuation. (a) is the pure elastic response; (b) and (c) are the viscoelastic responses for attenuation in the surficial layer only, and in both the surficial and overburden layers, respectively. (d) is the pure elastic response including scattering in the surficial layer; (e) and (f) are the responses of the same viscoelastic models used to compute (b) and (c), respectively, with the inclusion of the same scattering as in (d). Times are relative; the absolute zero-offset time is model dependent, but is approximately 1.29 s.

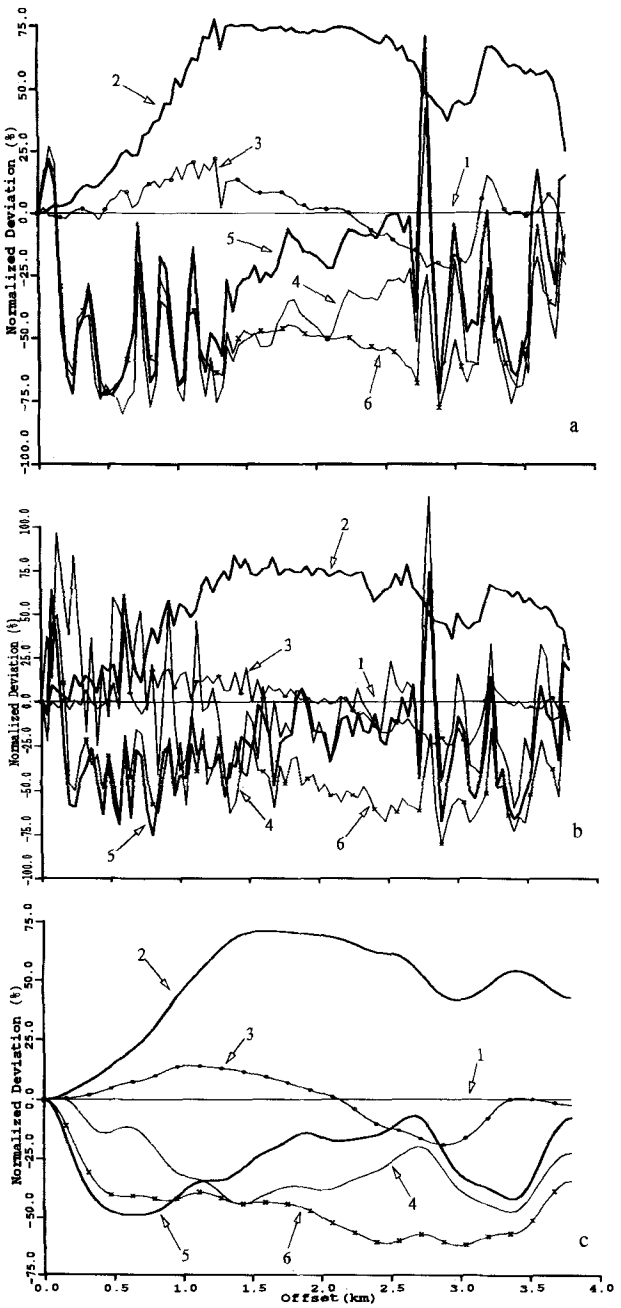


FIG. 9. AVO responses for six configurations with the geometry of model C in Figure 1. In (a), curves 1 through 6 correspond to the data in Figures 8a through 8f, respectively. In (b), curves 1 through 6 correspond to the same data without interference subtraction. (c) is the same as (b), but with smoothing prior to normalization.


Blair, D. P., 1990, A direct comparison between vibrational resonance and pulse transmission data from assessment of seismic attenuation in rock: Geophysics, **55**, 51–60.

Bourbié, T., and Nur, A., 1984, Effects of attenuation on reflections: Experimental test: J. Geophys. Res., **89**, 6197–6202.

Carcione, J. M., Kosloff, D., and Kosloff, R., 1988, Viscoacoustic wave propagation simulation in the earth: Geophysics, **53**, 769–777.

Castagna, J. P., 1993a, Petrophysical imaging using AVO: The Leading Edge, **12**, No. 3, 172–178.

——— 1993b, AVO analysis—Tutorial and review, *in* Castagna, J. P. and Backus, M. M., Eds., Offset dependent reflectivity: Theory and practice of AVO analysis: Soc. Expl. Geophys., Invest. Geophys. **8**, 3–36.

Castagna, J. P. and Backus, M. M., Eds., 1993, Offset dependent reflectivity: Theory and practice of AVO analysis: Soc. Expl. Geophys., Invest. Geophys. **8**.

Castagna, J. P., Batzle, M. L., and Kan, T. K., 1993, Rock physics—The link between rock properties and AVO response, *in* Castagna, J. P. and Backus, M. M., Eds., Offset dependent reflectivity: Theory and practice of AVO analysis: Soc. Expl. Geophys., Invest. Geophys. **8**, 135–171.

Castagna, J. P., Han, D. H., and Batzle, M. L., 1995, Issues in rock physics and implications for DHI interpretation: The Leading Edge, **14**, No. 8, 883–885.

Chacko, S., 1989, Porosity identification using amplitude variation with offset: Examples from South Sumatra: Geophysics, **54**, 942–951.

Chang, H., and McMechan, G. A., 1996, Numerical simulation of multiparameter scattering, Bull. Seis. Soc. Am., **86**, 1820–1829.

Chiburis, E. F., 1984, Analysis of amplitude versus offset to detect gas/oil contacts in the Arabian Gulf: 54th Ann. Internat. Mtg., Soc. Expl. Geophys., Expanded Abstracts, 669–670.

——— 1987, Studies of amplitude versus offset in Saudi Arabia: 57th Ann. Internat. Mtg., Soc. Expl. Geophys., Expanded Abstracts, 614–616.

——— 1993, AVO applications in Saudi Arabia, *in* Castagna, J. P. and Backus, M. M., Eds., Offset dependent reflectivity: Theory and practice of AVO analysis: Soc. Expl. Geophys., Invest. in Geophys. **8**, 211–229.

Chiburis, E. F., and Al-Faraj, M., 1987, Depthing shallow reflectors using postcritical *P*-wave reflection amplitudes: 57th Ann. Internat. Mtg., Soc. Expl. Geophys., Expanded Abstracts, 631–633.

Crossley, D. J., and Jensen, O. G., 1989, Fractal models in refraction seismology: Pure. Appl. Geophys., **131**, 61–76.

Dong, Z., and McMechan, G. A., 1995, 3-D viscoelastic anisotropic modeling of data from a multicomponent, multiazimuth experiment in northeast Texas: Geophysics, **60**, 1128–1138.

Drufuca, G., and Mazzotti, A., 1995, Ambiguities in AVO inversion of reflections from a gas-sand: Geophysics, **60**, 134–141.

Estill, R., and Wrolstad, K., 1993, Interpretive aspects of AVO—Application to offshore Gulf Coast bright-spot analysis, *in* Castagna, J. P. and Backus, M. M., Eds., Offset dependent reflectivity: Theory and practice of AVO analysis: Soc. Expl. Geophys., Invest. Geophys. **8**, 267–284.

Frankel, A., and Clayton, R. W., 1986, Finite-difference simulations of seismic scattering: Implications for the propagation of short-period seismic waves in the crust and models of crustal heterogeneity: J. Geophys. Res., **91**, 6465–6489.

Juhlin, C., and Young, R., 1993, Implications of thin layers for amplitude variation with offset (AVO) studies: Geophysics: **58**, 1200–1204.

Kan, T. K., and Young, C. Y., 1993, Prestack synthetic seismogram of finely layered elastic earth, *in* Castagna, J. P. and Backus, M. M., Eds., Offset dependent reflectivity: Theory and practice of AVO analysis: Soc. Expl. Geophys., Invest. Geophys. **8**, 93–102.

Kang, I. B., and McMechan, G. A., 1990, Two-dimensional elastic pseudo-spectral modeling of wide aperture seismic array data with application to the Wichita uplift–Anadarko Basin region of southwestern Oklahoma: Bull. Seis. Soc. Am., **80**, 1677–1695.

——— 1993a, Viscoelastic seismic responses of 2-D reservoir models: Geophys. Prosp., **41**, 149–163.

——— 1993b, Effects of viscoelasticity on seismic wave propagation in fault zones, near surface sediments and inclusions: Bull. Seis. Soc. Am., **83**, 890–906.

——— 1994, Separation of intrinsic and scattering $Q$ based on frequency-dependent amplitude ratios of transmitted waves: J. Geophys. Res., **99**, 23 875–23 885.

Kim, K. Y., Wrolstad, K. H., and Aminzadeh, F., 1993, Effects of transverse isotropy on *P*-wave AVO for gas sands: Geophysics, **58**, 883–888.

Koefoed, O., 1955, On the effect of Poisson's ratios of rock strata on the reflection coefficents of plane waves: Geophys. Prosp., **3**, 381–387.

Landro, M., Buland, A., and D'Angelo, R., 1995, Target-oriented AVO inversion from Valhall and Hod fields: The Leading Edge, **14**, No. 8, 855–861.

Luh, P. C., 1993, Wavelet attenuation and bright spot detection, *in* Castagna, J. P. and Backus, M. M., Eds., Offset dependent reflectivity: Theory and practice of AVO analysis: Soc. Expl. Geophys., Invest. Geophys. **8**, 190–198.

Martinez, R. D., 1993, Wave propagation effects on amplitude variation with offset measurements: A modeling study: Geophysics, **58**, 534–543.

Martinez, R. D., and McMechan, G. A., 1987, Analysis of absorption and dispersion effects in synthetic $\tau$–$p$ seismograms: Geophysics, **52**, 1033–1047.

——— 1991, $\tau$–$p$ seismic data for viscoelastic media—Part 2: Linearized inversion: Geophys. Prosp., **39**, 157–181.
Ostrander, W. J., 1984, Plane-wave reflection coefficients for gas sands at nonnormal angles of incident: Geophysics, **49**, 1637–1648.
Poley, J. P., 1964, Critical angle effects in seismic exploration: Geophys. Prosp., **12**, 397–421.
Reshef, M., Kosloff, D., Edward, M., and Hsiung, C., 1988, Three-dimensional elastic modeling by the Fourier method: Geophysics, **53**, 1184–1193.
Ross, C. P., 1991, Contamination and bias in AVO analysis: 61st Ann. Internat. Mtg., Soc. Expl. Geophys., Expanded Abstracts, 1066–1069.
——— 1992, Incomplete AVO near salt structures: Geophysics, **57**, 543–553.
Rutherford, S. R., 1993, Noise-discriminating statistical-amplitude compensation for AVO analysis: Geophysics, **58**, 1831–1839.
Rutherford, S. R., and Williams, H. R., 1989, Amplitude-versus-offset variations in gas sands: Geophysics, **54**, 680–688.
Samec, P., and Blangy, J. P., 1992, Viscoelastic attenuation, anisotropy and AVO: Geophysics, **57**, 441–450.
Sams, M. S., 1995, Attenuation and anisotropy: the effect of extra fine layering: Geophysics, **60**, 1646–1655.
Santoso, D., Alfian, Alam, S., Sulistiyono, Hendraya, L., and Munadi, S., 1995, Estimation of limestone reservoir porosity by seismic attribute and AVO analysis: Expl. Geophys., **26**, 437–443.
Schultz, P. S., Pieprzak, A. W., and Loh, E. K. L., 1983, A case for larger offsets: Geophysics, **48**, 238–247.
Shapiro, S. A., and Hubral, P., 1996, Elastic waves in finely layered sediments: The equivalent medium and generalized O'Doherty-Anstey formulas: Geophysics, **61**, 1282–1300.
Shapiro, S. A., Zien, H., and Hubral, P., 1994, A generalized O'Doherty-Anstey formula for waves in finely layered media: Geophysics, **59**, 1750–1762.
Shuey, R. T., 1985, A simplification of the Zoeppritz equations: Geophysics, **50**, 609–614.
Simmons, J. L., and Backus, M. M., 1994, AVO modeling and the locally converted shear wave: Geophysics, **59**, 1237–1248.
——— 1996, Waveform-based AVO inversion and AVA prediction error: Geophysics, **61**, 1575–1588.
Smith, G. C., and Gidlow, P. M., 1987, Weighted stacking for rock property estimation and detection of gas: Geophys. Prosp., **35**, 993–1014.
Snyder, A. G., and Wrolstad, K. H., 1992, Direct detection using AVO, Central Graben, North Sea: Geophysics, **57**, 313–325.
Sun, R., and McMechan, G. A., 1991, Depth-filtering for one-component data: Geophysics, **56**, 1482–1485.
Tal-Ezer, H., Carcione, J. M., and Kosloff, D., 1990, An accurate and efficient scheme for wave propagation in linear viscoelastic media: Geophysics, **55**, 1366–1379.
Tang, X., and Burns, D. R., 1992, Seismic scattering and velocity dispersion due to heterogeneous lithology: 62nd Ann. Internat. Mtg., Soc. Expl. Geophys., Expanded Abstracts, 824–827.
Todd, C. P., and Backus, M. M., 1985, Offset-dependent reflectivity in a structural context: 55nd Ann. Internat. Mtg., Soc. Expl. Geophys., Expanded Abstracts, 586–588.
Toksöz, M. N., Johnson, D. H., and Timur, A., 1979, Attenuation of seismic waves in dry and saturated rocks: 1. Laboratory measurements: Geophysics, **44**, 681–690.
Widmaier, M. T., Shapiro, S. A., and Hubral, P., 1994, Kirchhoff migration and AVO in the case of a thinly-layered overburden: 64th Ann. Internat. Mtg., Soc. Expl. Geophys., Expanded Abstracts, 934–936.
——— 1996, AVO correction for scalar waves in the case of a thinly-layered overburden: Geophysics, **61**, 520–528.
Winterstein, D. F., and Hanten, J. B., 1985, Supercritical reflections observed in $P$- and $S$-wave data: Geophysics, **50**, 185–195.
Xu, Y., Gardner, G. H. F., and McDonald, J. A., 1993, Some effects of velocity variation on AVO and its interpretation: Geophysics, **58**, 1297–1300.
Yu, G., 1985, Offset-amplitude variation and controlled-amplitude processing: Geophysics **50**, 2697–2708.